

Contents lists available at ScienceDirect

# Journal of Crystal Growth

journal homepage: www.elsevier.com/locate/jcrysgro





# Atomistic simulation solution of MBE epitaxy of 6.1-Å semiconductors multiple QW heterostructures

P.K. Saxena\*, P. Srivastava, A. Srivastava, A. Saxena

Tech Next Lab Pvt Ltd. Lucknow 226003. India

#### ARTICLE INFO

Communicated by: Lijun Liu

Keywords: EpiGrow Simulator TNL-TCAD Simulation Atomistic Defects

#### ABSTRACT

The authors present an atomistic approach aimed at replicating the real-time Molecular Beam Epitaxy (MBE) experiment of a Triple-Barrier Resonant Tunneling (TBRT) heterostructure, which is constructed from InAs/AlSb heterojunctions. This work is directed towards potential applications in CMOS-based memory by optimizing the thickness of various layers. The study investigates the impact of MBE reactor geometry and the kinetic Monte Carlo (kMC) method, which encompasses adsorption, diffusion, and desorption processes, all examined at an atomistic scale with precision at the level of individual deposited atoms. A thorough exploration of the energy barriers encountered during the deposition process is conducted, particularly in relation to the validation of experimental results published by Akihiro Ohtake's and Peter D. Hodgson's research groups [1],[3]. The Frankvan der Merwe growth mode was found to be the predominant mechanism during the growth phase. The growth morphology of the heterostructures is accurately replicated, providing a deeper understanding of the underlying physics associated with the atomistic phenomena in each material layer. The proposed technique allows for precise predictions of various output parameters, such as growth rate, defect types, their densities relative to position within the lattice, and layer-by-layer lattice parameters. Furthermore, the optimization of input parameters, based on the proposed generalized MBE epitaxy model, facilitates the thickness optimization of each material layer, ultimately leading to the development of high-performance devices. This technique has demonstrated its effectiveness in accelerating the MBE epitaxy process from development to production timelines.

#### 1. Introduction

The phenomena of the resonant tunneling proposed by Tsu and Esaki could be successfully realized in various materials, including semiconductors and oxides, with the advancement in the deposition techniques during the last few decades [3–7]. Most of the resonant tunneling diodes (RTDs) composed of a single quantum well layer sandwiched between two barrier layers utilizes the unusual band offset feature of the 6.1-Å semiconductor family (InAs, AlSb, and GaSb etc) to perform the quantum resonant tunneling mechanism [8]. The RTDs are mostly used for the development of the THz oscillators [9], logic elements [10] and high-sensitive detectors applications include the strain [11], temperature mapping [12]. The fine tuning of the quantum well thickness is essential requirement to development of these devices with enhanced performance. The MBE epitaxial deposition processes of III-V still require several issues to be addressed e.g. reproducibility of growth process, defects free high crystalline quality, strain etc. The growth of

complex hetero-structure devices based on the 6.1-Å semiconductor family also requires high accuracy throughout the growth associated with type I and II hetero-structure interfaces. However, the limitations imposed by lattice constant mismatch between constituent layers in different materials play a decisive role in generation of strained growth morphology of thin films. The experimental epitaxy process optimization to achieve high quality films requires lot of experimentation. Commercially available GaAs substrate is ideal for 6.1-Å semiconductor family epitaxy due to their thermal stability and crystalline quality, but challenges like lattice mismatches and thermal expansion differences complicate high-quality film production.

To address the aforementioned challenges, researchers have attempted various theoretical models, such as the precursor state model [13], the kinetic model [14], and thermodynamic modeling [15,16], aimed at predicting the nucleation and growth mechanisms involved in III-V Molecular Beam Epitaxy (MBE). However, these discussions are somewhat limited and fail to adequately account for the experimental

E-mail address: praveen@technextlab.com (P.K. Saxena).

<sup>\*</sup> Corresponding author.

data [13–16]. This is particularly true for group V elements, such as arsenic, where a significant proportion of  $As_4$  is present in the overall arsenic flux, resulting in varying  $As_2/As_4$  ratios. At present, there are no theoretical models for epitaxial growth that simultaneously consider reactor geometries and the different flux-dependent adsorption, hopping, and nucleation conditions necessary to investigate the atomistic-scale deposition process.

The article provides atomistic solution against the challenges associated with the MBE epitaxy process and presents various studies that have utilized theoretical techniques to reproduce different reactor-based epitaxy experiments. The references [17-21] provide insights into these studies. Reference (17) demonstrates the growth of II-VI materials (CdTe & HgCdTe) using the MBE reactor at temperatures ranging from 170-300 °C. Reference (18) reflects the MOCVD growth of GaAs at appropriate growth temperatures. References (19-20) elaborate on the MOCVD growth of III-V nitrides at higher growth temperatures. Reference (21) reflects the CVD growth of Si and SiGe at appropriate growth temperatures. Reproducibility of similar experiments is often a challenging and expensive endeavor for the industry. Differences in reactor geometry, substrate, and growth temperatures can generate varying growth morphologies. For instance, a similar MOCVD reactor used for the deposition of 6.1-Å semiconductors at 450–550 °C and III-V nitrides at 750-1400 °C. Although the deposition processes are the same, the gas- and surface-phase reaction kinetics, as well as the nucleation process, can lead to changes in the growth morphology (strain, defects, etc.). The proposed cost-effective predictive simulation technique enables users to optimize the input parameters to achieve high-quality films through real-time MBE growth experiments, potentially reducing the experimentation costs.

The present article demonstrates the MBE growth of 6.1-Å Semi-conductors via atomistic simulation technique; the basic algorithms/method of MBE reactor epitaxy simulation is shown in Fig. 1, except the input conditions that have been varied according to material systems used here. The reliability of proposed technique has been shown here through the output results which were found to be in excellent matching with the experiments under using real input conditions. Two separate Molecular Beam Epitaxy (MBE) deposition processes of 6.1-Å Semi-conductors, taken from reference [1] and [3] respectively, were reproduced through proposed simulation technique.

In the initial case study, the GaSb Molecular Beam Epitaxy (MBE) process on a GaAs (111) substrate was successfully validated [1]. The positive outcomes of this experimental validation have prompted further exploration into the intricate multilayer TBRT hetero-structure epitaxy processes, including an examination of each interface in the subsequent case study, as referenced in [3]. This paper presents an instance where the optimization of the MBE process is achieved through atomistic simulation. This approach facilitates the attainment of a balance between growth rate and crystal quality. The proposed simulation methodology can be employed to optimize input parameters prior to actual experimentation, thereby minimizing the consumption of raw materials, resources and manpower, as well as expediting development timelines.

#### 2. Computational details

The MBE deposition algorithms of deposition inbuilt in the TNL-EpiGrow simulator is depicted in Fig. 1. It exploits inhouse developed kinetic Monte Carlo (kMC) technique, detailed in reference [17]. The TNL-MBE simulator is an advanced atomistic deposition technique that operates without initial assumptions or predefined parameters. It replicates the MBE growth process as in real MBE reactor by heating elements in a valved cracker cells, maintaining equilibrium vapor pressure, and allowing vapor to escape, creating a material flux with a Maxwell-Boltzmann velocity distribution [17].

$$J = 1.12 \times 10^{22} \frac{Sp}{\frac{1}{DMT^{1/2}}} \tag{1}$$

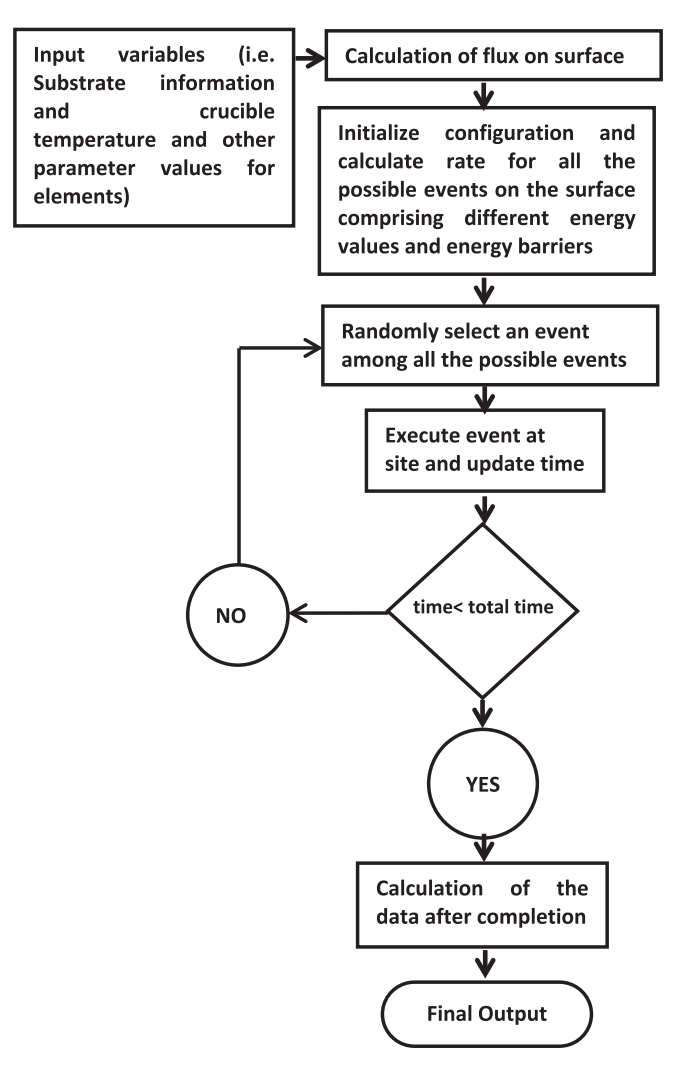


**Fig. 1.** The deposition and various parameters extraction algorithms flow chart inbuilt the TNL-EpiGrow simulator.

here, J is the molecular flux (molecules/cm $^2$ -s), p is the vapor pressure (kPa), M, T and S are the molecular weight (amu), temperature (K), the exit aperture area respectively. l is the distance from the aperture to the substrate. The vapor pressure (p) is dependent on the crucible temperature and the material's atomic number.

$$log(p/atm) = A + B/T + C*log(T) + D/T^3$$
(2)

The Eq. (2) predicts vapor pressures within  $\pm~5~\%$  and determines the vapor pressure of metallic elements in solid state in range of  $10^{-15}-10^{-3}$  atm. Coefficients A, B, C, and D, along with melting points and phases, are provided in Table 1 for 6.1 family semiconductors. Alloys containing group V elements, such as As, P and Sb, generally do not display a direct correlation between their composition and the ratio of the incoming fluxes. Using the  $As_2/As_4$  and  $Sb_2/Sb_4$  ratios through valved cracker cells at various substrate temperatures, the arsenic and antimony fluxes are optimized here. However, group III elements are observed as a linear function of the ratio between the incident group III element fluxes.

At the substrate surface, the incoming atoms flux of the source materials undergoes a number of processes. The atoms bonding is decided different energy values and hybridization rule in which atom itself find the bonding position following the natural phenomenon of the growth process as in the real reactor environment. The surface grows like an actual sample with atoms taking position according to their bond angles

**Table 1**Coefficients A, B, C, D along with their melting point and phase.

Atomic Number	Elements	Α	В	С	D	<b>Melting Point</b>	Phase
13	Al	9.459	-17342	-0.7927	0	933	Solid
31	Ga	6.657	-14208	0	0	302.9	Solid
33	As	-66.878	-1105.12	22.27	0	889	Solid
49	In	5.991	-12548	0	0	429	Solid
51	Sb	10.571	-10300	0	0	903.78	Solid

and distances. The capabilities to map each and every deposited atom over the lattice layer-by-layer make it possible to extract lattice parameters, mole fraction, strain, edge dislocations, vacancies, and interstitial defect density along with the roughness [17].

The kinetic Monte Carlo (kMC) algorithm calculates the overall rate (R) associated with the adsorption (A), diffusion (H), and desorption (D) processes [17]:

$$R = A + H + D \tag{3}$$

here, A = FLW,  $H = \sum_j D_0 e^{\frac{-E_j}{k_B T}}$  and  $D = \sum_j D_0 e^{\frac{-E_{dej}}{k_B T}}$  are the total adsorption, diffusion and desorption rates respectively. The F is the incoming flux, L and W denote the length and width of the square shaped substrate respectively. The  $E_j$  represents hopping activation energy and  $E_{desj}$  is the desorption activation energy of the  $j^{th}$  atom respectively.

Any event (i.e. adsorption (A), hopping (H) or desorption (D)) in kMC process is selected randomly, but it is heavily dependent on the total rate and which ultimately rely on different energies associated with hopping atoms. These different energies include Schwoebel energy ( $E_{\rm shw}$ ) and incorporation energy ( $E_{\rm i}$ ) which act as barriers, nearest neighbor energy ( $E_{\rm n}$ ) and surface energy ( $E_{\rm s}$ ) among adatoms. The Ehrlich–Schwoebel barrier ( $E_{\rm shw}$ - a diffusion barrier, encountered by a surface atom, when crossing an atomic down step.) and incorporation energy ( $E_{\rm i}$ ) are the ascending (up step) barrier energies used for movement of atoms over the lattice. Each type of III and V group atoms and molecules have been given due consideration in the method. These energy parameters of different III/V systems are depicted in Table 2. Activation energies vary by material type, with bonds forming only between adjacent atoms [17–23];

$$E = E_s + n.E_n \tag{4}$$

here,  $E_s$  is the energy barrier for surface diffusion,  $E_n$  is the binding energy of nearest atoms, and n is the number of nearest neighbors (nn) on the surface, defining the overall activation energy. These step barriers significantly influence surface diffusion process, affecting the overall activation energy of an atom for hopping.

$$E = \begin{cases} E_s + nE_n + E_{shw} \\ E_s + nE_n + E_i \end{cases}$$
 (5)

The number of atoms surrounding an atom decides the hopping energy and obviously the more the nearest neighbor atoms, the less probable the hopping event is. Also, if there is no neighbor site vacant for an atom to hop, the atom is trapped to the position until either some atom move from the nearby position or that site become the permanent

binding site for that particular atom. Similarly, an atom hopping to a site depend on Schwoebel  $(E_{\text{shw}})$  and incorporation  $(E_i)$  barriers  $(Eq.\ (5),$  which obviously chose a site approached with minimum efforts. The Schwoebel and incorporation energy barriers are destination dependent. However, the activation energy for the same atom is also dependent on the diffusion destination. At the substrate surface, incoming atoms can either be physiosorbed, loosely attached via van der Waals forces, or chemisorbed, strongly bonded through chemical interactions. For an atom to integrate into the lattice, it must first become chemisorbed at a specific site, with the incorporation rate indicating the speed of this process. Atoms and molecules can move across the surface, desorb into the vacuum, or enter the crystal structure, while interactions among adatoms may break down larger molecules.

The capability to trace each deposited atom with its position over the lattice make it possible to measure the distances of each atom in each monolayer with their neighbors in the both vertical and lateral directions,. Taking average of these distances generate each monolayer lattice parameters (a and c). Further, taking the average of a and c values of various monolayer of each type material system generate overall 'a' and 'c' values. The strain,  $\in$ , (both in vertical and lateral directions) is computed using the 'a' and 'c' values. The strain in the plane of each hetero-interface is calculated through the extracted lattice parameters.

$$\epsilon = \frac{a_s - a_0}{a_0} \tag{6}$$

here,  $a_0$  is the extracted average lattice parameter of substrate or beneath monocrystalline layer over which deposition is done.  $a_s$  is the lattice parameter of the depositing materials monolayer. Both types of compressible and tensile strain components can be easily extracted.

#### 3. Results and discussion

This paper presents two case studies on MBE deposition processes of InAs, GaSb, and AlSb taken from references [1] and [3]. The input process parameters are listed in Table 2. The first study verifies the GaSb MBE epitaxy on GaAs (111), with simulated results aligning well with experimental data [1,2]. This success led to further investigation of the multilayer TBRT hetero-structure in the second study [3]. Both simulation case studies yielded results consistent with experimental findings, showing strong correlations in key parameters like growth rate, lattice parameter, dislocation density, and mole fraction. Various energy barriers, such as Schwoebel, incorporation, and desorption energy, different energies e.g. nearest neighbor, surface, significantly influence the atomic bonding and growth modes, governing surface kinetics. Their

**Table 2** Input Process Parameters.

Case Study	<b>Growth Steps</b>	Orfice Area (cm²)	Cell distance from substrate (cm)	Sticking Coeff	T <sub>sub</sub> (°C)	E <sub>s</sub> (eV)	E <sub>sch</sub> (eV)	E <sub>n</sub> (eV)	E <sub>d</sub> (eV)
Ist	GaSb	0.002	15	1	430	2.0	0.11	0.1	
IInd	AlSb	0.002	15	1	490	2.05	0.13	0.12	3.0
	GaSb				515	1.95	0.12	0.11	
	InAs				435	1.98	0.1	0.11	
	AlSb				515	2.01	0.12	0.12	
	InAs/AlSb/InAs/AlSb/				435	As above	:		
	InAs								

values were optimized by running the number of simulations to accurately predict experimental growth morphology.

The growth simulation of GaSb in first study was initiated by simultaneously incoming flux of the Ga and Sb, with Sb<sub>4</sub>/Ga flux ratio of ~4, over the GaAs (111) substrate under ultra-high vacuum condition of  $5\times 10^{-10}$  Torr on the GaAs (111) substrate at temperature 430  $^{\circ}\text{C}$  [1]. The significant contribution of different energy barriers (e.g. nearest neighbor, surface, Schwoebel, incorporation and desorption energy used here as the fitting parameters) was observed to play significant role in deciding the atom bonding and type of growth mode. These energy barriers control the surface kinetics at the surface. Their values were optimized to reproduce the experimental growth morphology. The surface profile has been extracted to distinguish among the type of growth mode. The growth mode profiles comparison after 2ML, 5ML and 10ML of GaSb over GaAs substrate is shown in Fig. 2a, b and c respectively. It is clearly reflected from the growth profiles that the deposition occurred in layer-by-layer mode. The small lattice mismatch among the 6.1-Å semiconductor family was responsible for the layer-bylayer mode and justified the experimental Frank-van der Merwe (FM) growth mode. The inter-planar spacing in the directions normal to the growth surface of the grown GaSb film (300 nm-thick) was calculated using the extracted lattice parameter 'a'. The inter-planner spacing values are estimated as;

$$d_{111} = a\sqrt{\frac{2}{3}} \tag{7}$$

The comparison of experimental data taken from reference [1] and extracted inter-planar spacing  $(d_{111})$  using Eq. (7), is depicted in Fig. 3. It is evident that the lattice constant of GaSb remains nearly constant despite an 8 % mismatch with the GaAs substrate. This phenomenon is attributed to the interfacial misfit array, which effectively alleviates the lattice strain on the GaSb layer at the GaSb/GaAs interface. Since the inplane lattice of 13 GaSb sites corresponds to 14 GaAs sites, a nearly instantaneous relaxation occurs in the GaSb layer, resulting in the lattice constant being maintained at a similar value, as noted in references [1,2]. The TNL-EpiGrow simulator is designed to measure the total dislocation density that arises from both planar and vertical lattice mismatches. The differentiation among various types of dislocations is currently under development. The excellent matching of lattice parameter justifies the reliability of the proposed simulation technique to successfully reproduce the MBE epitaxy experiment. The extracted growth rate  $\sim$  3.1 Å/s was found to be in good agreement with that of the experiment (0.3 nm/s) [1]. The edge dislocation density in the 24 ML-GaSb film grown though simulation was observed by tracing each

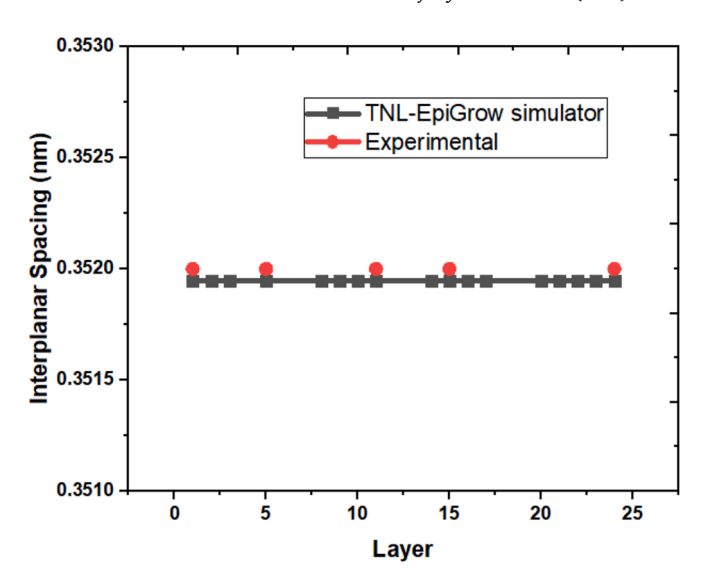


Fig. 3. The lattice constants of 300 nm-thick GaSb (111) films in the direction normal ( $d_{111}$ ) to the surface as a function of the monolayers. The black line represents output from TNL-EpiGrow simulator and red spheres are the experimentally extracted values [1].

deposited atom on the substrate, which is of the order of  $\sim 3.55 \times 10^9$  cm $^{-2}$ . It was also found in the range of that of experiment [1,2]. Though, there is still room for improvement by further optimizing the different energy barriers.

In second case study, the MBE epitaxy process based on an experimental Triple-Barrier Resonant Tunneling (TBRT) hetero-structure including two quantum wells and three barriers was reproduced through proposed atomistic simulation technique. The sequential deposition of InAs and AlSb were simulated on the buffer layer of GaSb grown over GaAs (111) substrate. The square shape substrate with dimension 60unitcell × 60unitcell of GaAs was taken. The input conditions were taken from reference [3] to reproduce the real-time MBE epitaxy experiment. The various energy barriers values were again optimized to reproduce the experimental growth morphology. To achieve the high crystalline films, the incoming flux i.e. As<sub>4</sub>/In, As<sub>4</sub>/In and Sb<sub>2</sub>/Al, Sb<sub>4</sub>/Al was optimized through minor variations in the effusion cell temperature under the MBE reactor environment. MBE growth simulation was conducted under conditions rich in group V elements, utilizing arsenic and antimony cracker cells. The incident fluxes of

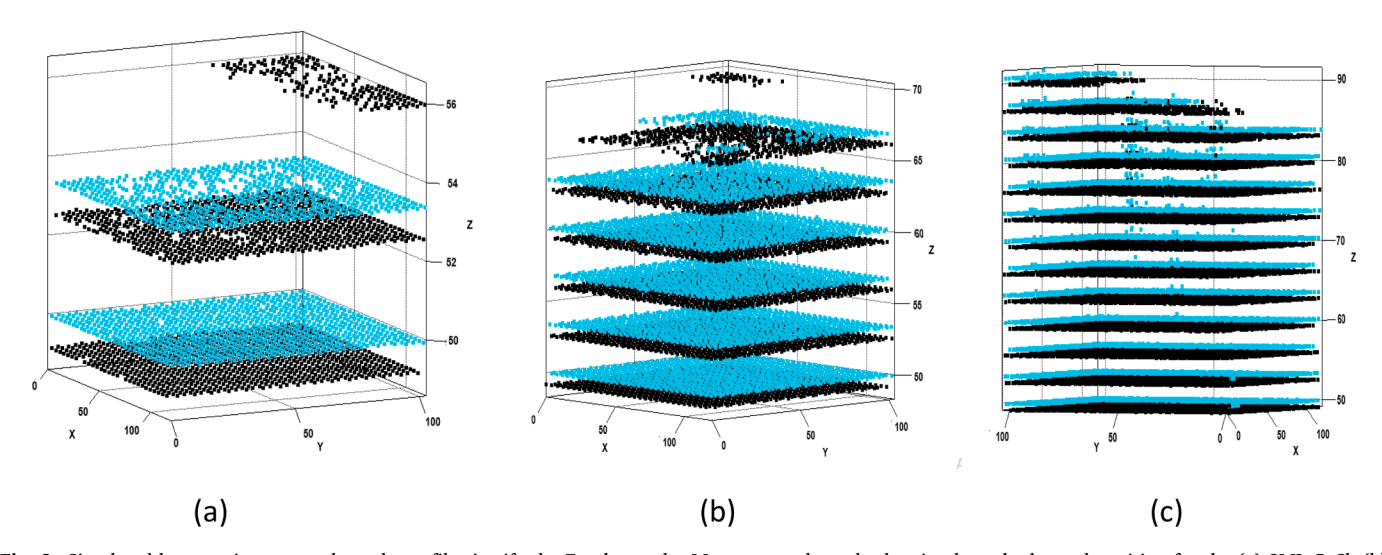
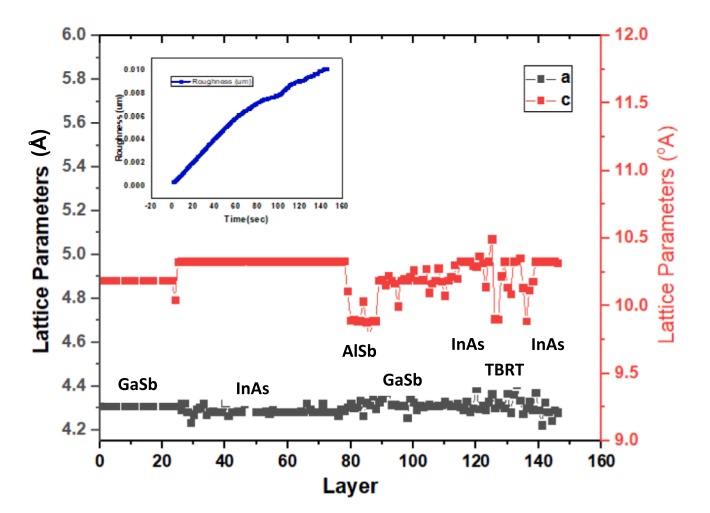


Fig. 2. Simulated heteroepitaxy growth mode profiles justify the Frank-van der Merwe growth mode showing layer-by-layer deposition for the (a) 2ML-GaSb (b) 5ML-GaSb (c) 10ML-GaSb over the GaAs(111) substrate.

arsenic and antimony comprised molecules such as  $As_2$ ,  $As_4$ ,  $Sb_2$ , and  $Sb_4$ , respectively. Typically, alloys that include group V elements like arsenic and antimony do not exhibit a straightforward relationship between their composition and the ratio of incoming fluxes of these elements. In contrast, the group III elements demonstrate a linear relationship with the ratio of the incident fluxes of group III elements. This study optimizes the arsenic and antimony fluxes by examining the ratios of  $As_2/As_4$  and  $Sb_2/Sb_4$  through valved cracker cells at various substrate temperatures. The minor temperature variation considered here is attributed due to the difference between actual MBE environment and simulation conditions.

The substrate temperature was taken constant over the entire substrate region. However, there is flexibility to include temperature gradient over the substrate in the TNL-EpiGrow simulator. The each deposited atom's position on the lattice was extracted, it has provided the direct access to the various unknown information associated with the growth, which is difficult to extract through sophisticated instruments. The 3D schematic view of Triple-Barrier Resonant Tunneling (TBRT) hetero-structure at the atomistic scale is depicted in Fig. 4. The thickness of each material layer given in reference [3] was matched, hence the growth rate. The extracted QW thickness is observed uniform in each layer in each direction.

The variation in extracted lattice parameters 'a' and 'c' are depicted in Fig. 5. The extracted lattice parameter 'a' remained almost constant and small variations are observed at each interface of the entire heterostructure grown. In each case study presented in the manuscript, a GaSb substrate with an orientation of  $\langle 111 \rangle$  is utilized. Ideally, both GaSb (100) and InAs exhibit a zinc-blende cubic structure, which implies that the "a" and "c" constants should be identical. According to Eq. (7), the extracted planar lattice parameter (d<sub>111</sub>) supports the occurrence of strain generation and the formation of dislocation phenomena at each interface during the deposition process, as evidenced by the interfacial misfits reported in references [1,2]. However, the parameter 'c' reflects variations at each hetero-interface. For the GaSb buffer layer, both lattice parameters 'a' and 'c' showed no variation, except at the GaSb/n-InAs interface, where alterations in the values of 'a' and 'c' were observed. The average lattice parameters for GaSb and InAs were determined to be 'a<sub>GaSb</sub>' = 4.31045 Å, 'a<sub>InAs</sub>' = 4.28598 Å, 'c<sub>GaSb</sub>' = 10.1899 Å, and ' $c_{InAs}$ ' = 10.33088 Å. A compressible strain was generated at the interface due to a  $\sim$ 3 % discrepancy in 'a' values. Direct



**Fig. 5.** Variation in the extracted lattice parameter "a" and "c" layer-by-layer profile of multi-steps InAs, AlSb, GaSb layers deposition on GaSb substrate, based on the heterostructure presented in reference [3]. The RMS roughness profile of RTD hetero-structure, extracted every second is shown in the inset diagram.

evidence of a clearly defined interfacial misfit dislocation network has been observed at the GaSb/GaAs(111) interface. Observations indicated that Ga atoms preferentially diffused into the InAs layers at the interface, especially near layer 25 along the x-axis, resulting in an In<sub>0.66</sub>Ga<sub>0.33</sub>As layer. The incorporation of Ga detail is crucial as it alters the band structure and may enhance device performance. The stress persisted until the 50th deposited monolayer, gradually decreasing until it reached the InAs/AlSb interface (layer 78). At this interface (layer 79), 2 % of Sb atoms were integrated into the InAs layers, forming a phase akin to InAsSb. This Sb incorporation is also evidenced by the significant change in the 'c' parameter values shown in Fig. 5, indicating a notable alteration in the crystal structure due to Sb presence. The average lattice parameters for AlSb were determined to be 'a' = 4.32503 Å and 'c' = 9.88265 Å, which further highlights the differences in lattice dimensions across the various layers. The detection of gallium (Ga) and antimony (Sb) atoms within the 50 nm-InAs layer at the interfaces of GaSb/n-InAs

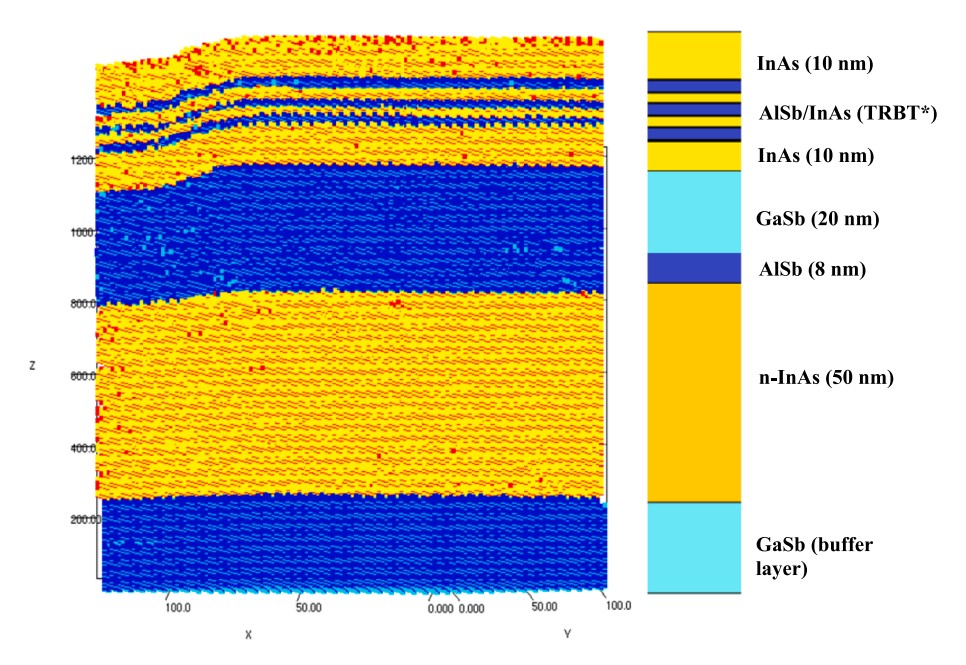


Fig. 4. Schematic view of reproduced RTD hetero-structure, refer to reference [3], grown using TNL-EpiGrow simulator. Atomistic layer-by-layer profile of (Al-Blue, Ga-Blue, Sb—Cyan, In—Yellow and As—Red spheres) showing different material layers with their extracted thickness.

and InAs/AlSb provided significant evidence for the upward and downward diffusion of these atoms during the growth processes simulation. This diffusion phenomenon indicates that the atomic movement is not only occurring within the layers themselves but also across the interfaces, which can have implications for the electronic and structural properties of the materials involved. At the AlSb/GaSb hetero-interface, specifically at the 88th deposited layer, the formation of the Al<sub>0.3</sub>Ga<sub>0.7</sub>Sb phase was identified. This phase formation is critical as it suggests a compositional change at the interface, which can influence the overall material properties. Notably, only minimal changes were observed in the lattice parameters, specifically the 'a' and 'c' parameters, indicating that while a new phase are forming, the structural integrity of the surrounding materials remains largely intact. In contrast, an analysis of the GaSb/InAs hetero-interface at deposited layer 112 revealed a different scenario. Here, a variation in the 'c' parameter was noted, suggesting that the vertical lattice spacing is affected, possibly due to the interaction between the GaSb and InAs layers. However, the 'a' parameter, which corresponds to the in-plane lattice spacing, remained nearly unchanged. This discrepancy between the 'a' and 'c' parameters could imply that the atomic arrangement in the plane of the layers is stable, while the vertical arrangement is more susceptible to changes, potentially due to the differing atomic sizes and bonding characteristics of the materials involved. Overall, these findings highlight the complex interplay of atomic diffusion and phase formation at the interfaces of these semiconductor materials. Understanding these interactions is crucial for optimizing the performance of heterostructures in advanced semiconductor technologies. In examining the overall variation of the lattice parameter 'a' throughout the TBRT hetero-structure, including at each hetero-interface, it has been observed that these changes are minimal. This stability in the lattice parameter is crucial as it contributes to the uniformity of the material properties across the structure. The minimal variation in 'a' results in a reduction of in-plane strain within the hetero-structure justify the experimental observation refer to reference [2,3].

The variation observed in root mean square (RMS) roughness values extracted after each second deposition is shown in satellite figure of Fig. 5. The roughness curve has shown dependence on the variation of lattice parameter 'a'. Initially for few material layers (GaSb, n-InAs, and AlSb), it increased with the growth time due variation in lattice parameters. However, a small drop was observed at the hetero-interface AlSb/GaSb. The in-plane lattice parameter slightly value decreased in case of hetero-interface AlSb/GaSb, clearly reflected from in-plane lattice parameter curve. The atomic radii of Al and Ga atoms are responsible slight decrease in roughness values as  $R_{Al} > R_{Ga}$ . The compressive strain relieved itself at the hetero-interface AlSb/GaSb and allowed the deposition at smoother surface in layer-by-layer mode, hence the roughness values decreased. This drop around the 90 s, i.e. AlSb(8 nm)/ GaSb (20 nm) interface is attributed due difference in group III element radius. The atomic radii of Al atoms ( $R_{Al} = 1.43 \text{ Å}$ ) are greater than that of Ga atoms ( $R_{Ga} = 1.35 \text{ Å}$ ). The big radii Al deposited atoms generate irregular surface and suddendly the material flux transition occurs, the low radii Ga atoms flux deposited over the irregularities present over the AlSb layer, surface smoothness increases. Hence, the RMS value decreases in GaSb material layer as compared to AlSb layer until the GaSb/ In As interface reached. However, the 'a $_{\text{In As}}$ ' matches itself with the beneath layer 'a<sub>GaSb</sub>', therefore further increase in roughness value is observed, The roughness value increased for the  $\sim\!2$  nm thick AlSb (barrier) and slightly decreased for the  $\sim$ 2 nm thick InAs (quantum well) layers due to increase in-planar lattice parameters. However, the lattice mismatch between them almost remained 8 %. The RMS value shows small drop around 90 s.

The strain characteristics derived from simulations of the GaSb/InAs/AlSb layers deposition on GaAs(111) substrate employed in this context elucidate the well-documented phenomena that promote the recombination and termination of threading dislocations. In-plane strain leads to the formation of defects, such as threading dislocations. The

variation in dislocation density layer-by-layer in each material system is shown in Fig. 6. The high value of dislocation density is observed at GaAs/GaSb interface. The dislocation density reduces as the growth advances in the vertical direction. However, the minimum dislocation density observed at GaSb/InAs interface and justifies the observation of RMS roughness. The reduction in in-plane strain is further corroborated by the measured average dislocation density within the entire TBRT hetero-structure, which is approximately  $\sim 10^{10}$  cm<sup>-2</sup>. This relatively high dislocation density against the experimentally ECCI-measured surface defect density  $\sim$  (2.1  $\pm$  0.1)  $\times$  10<sup>8</sup> cm<sup>-2</sup>, indicates that the material quality is high. The difference of two (02) order in extracted average edge dislocation density values obtained via simulation against the experimentally ECCI-measured values are attributed due to annealing effect. The experimental film has been first cooled then annealed for recrystallization and reduction of dislocations take place. However, the extracted dislocation density is directly measured from the film without any recrystallization process.

The generation of point defects (vacancies) was observed to depend on the strain on a layer-by-layer basis, refer to Fig. 7. The number of vacancy generation in InAs material layer is almost double of bulk GaSb. The vacancy further decreases in AlSb and it increase almost double in GaSb layer. At GaSb/InAs interface, it again decreases. Similar, pattern is observed in InAs/AlSb quantum wells and barriers layers. The reason is attributed due to difference in group III and V elements atomic radii. Moreover, the analysis of the vacancy density across the entire heterostructure reveals that it is also low, estimated at around  $\sim\!2$  % of the total number of deposited atoms. A low vacancy density is indicative of a well-ordered crystal structure, which is essential for achieving optimal electronic properties in semiconductor devices.

#### 4. Conclusion

The major aim of the current research is to achieve successful reproduction of Molecular Beam Epitaxy (MBE) process of complex heterostructure growth morphology and its output characteristics, utilizing a proposed generalized atomistic simulation technique in form commercial simulator. This approach offers a cost-effective solution for simulating the MBE reactor-based epitaxy process for the 6.1-Å semiconductor family, applicable to various technological needs, such as the bulk epitaxy of GaSb on a GaAs (111) substrate and the development of Triple-Barrier Resonant Tunneling (TBRT) heterostructures with proper understanding of group flux through cracker cells. This research provides a deeper insight into the deposition phenomena occurring within

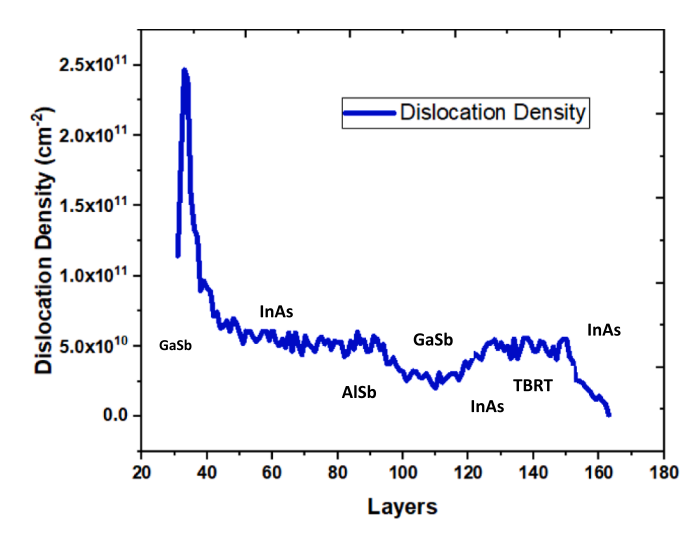


**Fig. 6.** Variation in the extracted dislocation density layer-by-layer profile of reproduced multi-steps RTD hetero-structures (InAs, AlSb, GaSb layers deposition on GaSb substrate) as reported in reference [3].

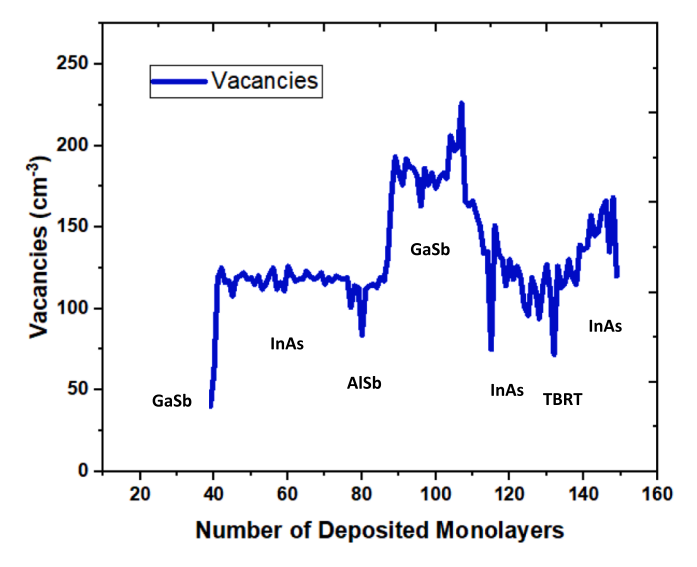


**Fig. 7.** Variation in the extracted vacancies layer-by-layer profile of reproduced RTD hetero-structure based on reference [3].

the reactor at the atomistic scale. The results demonstrate that the strain caused by the considerable vertical lattice mismatch at each interface between these materials is effectively mitigated through the creation of edge dislocations and vacancies. The proposed model serves as a valuable design guideline for engineers involved in the epitaxy process. The experimentation cost along with the technology development to production time cycle can be greatly reduced by using proposed technique in form of the TNL-EpiGrow simulator. The reactor manufacturers can use present model to calibrate the reactor parameters.

### CRediT authorship contribution statement

P.K. Saxena: Writing – review & editing, Writing – original draft, Validation, Supervision, Software, Methodology, Conceptualization. P. Srivastava: Validation, Software, Methodology. A. Srivastava: Methodology, Software, Validation. A. Saxena: Writing – review & editing, Writing – original draft, Validation, Supervision, Software, Methodology, Conceptualization.

#### Declaration of competing interest

The authors declare that they have no known competing financial interests or personal relationships that could have appeared to influence the work reported in this paper.

## Data availability

Data will be made available on request.

#### References

A. Ohtake, T. Mano, K. Mitsuishi, Y. Sakuma, Strain relaxation in GaSb/GaAs(111)
 A heteroepitaxy using thin InAs interlayers, ACS Omega 3 (2018) 15592, https://doi.org/10.1021/acsomega.8b02359.

- [2] M.D. Nordstrom, T.A. Garrett, P. Reddy, J. McElearney, J.R. Rushing, K.D. Vallejo, K. Mukherjee, K.A. Grossklaus, T.E. Vandervelde, P.J. Simmonds, Direct integration of GaSb with GaAs(111)A using interfacial misfit arrays, Cryst. Growth Des. 23 (12) (2023) 8670–8677, https://doi.org/10.1021/acs.cgd.3c00812.
- [3] P.D. Hodgson, D. Lane, P.J. Carrington, E. Delli, R. Beanland, M. Hayne, ULTRARAM: a low-energy, high-endurance, compound-semiconductor memory on silicon, Adv. Electron. Mater. 8 (2022) 2101103, https://doi.org/10.1002/ selm\_202101103
- [4] R. Tsu, L. Esaki, Tunneling in a finite superlattice, Appl. Phys. Lett. 22 (1973) 562, https://doi.org/10.1063/1.1654509.
- [5] L.L. Chang, L. Esaki, R. Tsu, Resonant tunneling in semiconductor double barriers, Appl. Phys. Lett. 24 (1974) 593, https://doi.org/10.1063/1.1655067.
- [6] K. Shono, H. Kawano, T. Yokota, M. Gomi, Effect of electron injection at the Pt-interface on a bipolar resistance switching device with Ta/Pr<sub>0.7</sub>Ca<sub>0.3</sub>MnO<sub>3</sub>/Pt structure, Appl. Phys Express 1 (2008) 55002, https://doi.org/10.1143/APFX 2 071401
- [7] H. Ikeda, M. Iwasaki, Y. Ishikawa, M. Tabe, Resonant tunneling characteristics in SiO<sub>2</sub>/Si double-barrier structures in a wide range of applied voltage, Appl. Phys. Lett. 83 (2003) 1456, https://doi.org/10.1063/1.1603352.
- [8] W.S. Choi, S.A. Lee, JH. You, S. Lee, HN. Lee, Resonant tunnelling in a quantum oxide superlattice, Nat. Commun. 6 (2015) 7424, https://doi.org/10.1038/ promms8424
- [9] F. Rothmayr, A. Pfenning, C. Kistner, J. Koeth, G. Knebl, A. Schade, S. Krueger, L. Worschech, F. Hartmann, S. Höfling, Mid-infrared GaSb-based resonant tunneling diode photodetectors for gas sensing applications, Appl. Phys. Lett. 112 (2018) 161107, https://doi.org/10.1063/1.5025531.
- [10] JP. Sun, G.I. Haddad, P. Mazumder, J.N. Schulman, Resonant tunneling diodes: models and properties, Proc. IEEE. 86 (1998) 641, https://doi.org/10.1109/ 5.663541
- [11] B. Petrović, A. Bader, J. Nauschütz, T. Sato, S. Birner, R. Weih, F. Hartmann, S. Höfling, 5.0 μ m emitting interband cascade lasers with superlattice and bulk AlGaAsSb claddings, J. Vac. Sci. Technol. B 42 (2024), https://doi.org/10.1116/ 6.0003584.
- [12] J. Li, H. Guo, J. Liu, et al., GaAs-based resonant tunneling diode (RTD) epitaxy on Si for highly sensitive strain gauge applications, Nanoscale Res. Lett. 8 (2013) 218, https://doi.org/10.1186/1556-276X-8-218.
- [13] T. Nomura, H. Ogasawara, M. Miyao, M. Hagino, Composition control of GaAsP grown by molecular beam epitaxy, J. Crystal Growth 111 (1991) 61, https://doi.org/10.1016/0022-0248(91)90947-4.
- [14] B.W. Liang, C.W. Tu, A kinetic model for As and P incorporation behaviors in GaAsP grown by gas-source molecular beam epitaxyJ, Appl. Phys. 74 (1993) 255, https://doi.org/10.1063/1.354155.
- [15] A.Y. Egorov, A.R. Kovsh, V.M. Ustinov, A.E. Zhukov, P.S. Kopev, C.W. Tu, A thermodynamic analysis of the growth of III–V compounds with two volatile group V elements by molecular-beam epitaxy, J. Crystal Growth 188 (1998) 69, https://doi.org/10.1016/S0022-0248(98)00043-8.
- [16] Z.-B. Hao, Z.-Y. Ren, W.-P. Guo, Y.i. Luo, Studies on incorporation of As2 and As4 in III–V compound semiconductors with two group Velements grown by molecular beam epitaxy, J. Cryst. Growth 224 (2001) 224–229, https://doi.org/10.1016/ S0022-0248(01)01019-3
- [17] P.K. Saxena, P. Srivastava, A. Srivastava, Defect analysis of MBE reactor-grown HgCdTe on Si, GaAs, GaSb, and CZT substrates through the TNL-Epigrow simulator, J. Electron. Mater. 53 (2024) 5803, https://doi.org/10.1007/s11664-024-11082-0.
- [18] PK. Saxena, P. Srivastava, R. Trigunayat, An innovative approach for controlled epitaxial growth of GaAs in real MOCVD reactor environment, J. Alloy. Compd. 809 (2019) 15175, https://doi.org/10.1016/j.jallcom.2019.151752.
- [19] P.K. Saxena, P. Srivastava, A. Srivastava, Dislocations/defects analysis in III-V nitrides a cost effective MOCVD epitaxy solution, J. Cryst. Growth 630 (2024) 127584, https://doi.org/10.1016/j.jcrysgro.2024.127584.
- [20] P.K. Saxena, P. Srivastava, A. Srivastava, MOCVD/MOVPE epitaxy of group III-V nitride with atomistic prospective & cost effectiveness, J. Cryst. Growth 650 (2025) 127975, https://doi.org/10.1016/j.jcrysgro.2024.127975.
- [21] P.K. Saxena, P. Srivastava, A. Srivastava, A. Saxena, Atomistic insights into predictive in silico chemical vapor deposition, Mater. Adv. 5 (2024) 2110, https:// doi.org/10.1039/d3ma01033c.
- [22] User Manual, TNL-EpiGrow Simulator, (2025), Tech Next Lab Private Limited. https://www.technextlab.com/epi\_g.html.
- [23] P.K. Saxena, P. Srivastava, Anshika Srivastava, Anshu Saxena, Uncovering the influence of nitridation on the dislocation density at atomistic scale in IIINitrides MOCVD/MOVPE epitaxy process, Sci. Rep. 15 (2025) 12630.